RESEARCH ARTICLE | DECEMBER 19 2022

Effect of dissolved gas on the tensile strength of water ⊘

Special Collection: Cavitation

Saikat Mukherjee 🕶 🔟 ; Hector Gomez



Physics of Fluids 34, 126112 (2022) https://doi.org/10.1063/5.0131165





CrossMark





Effect of dissolved gas on the tensile strength of water

Cite as: Phys. Fluids 34, 126112 (2022); doi: 10.1063/5.0131165 Submitted: 18 October 2022 · Accepted: 30 November 2022 · Published Online: 19 December 2022







Saikat Mukherjee^{a)} (ib) and Hector Gomez



AFFILIATIONS

School of Mechanical Engineering, Purdue University, 585 Purdue Mall, West Lafayette, Indiana 47907, USA

Note: This paper is part of the special topic, Cavitation.

a) Author to whom correspondence should be addressed: mukher32@purdue.edu

ABSTRACT

While theoretical estimates suggest that cavitation of water should occur when pressure falls much below -25 MPa at room temperature, in experiments, we commonly observe conversion to vapor at pressures of the order of 3 kPa. The commonly accepted explanation for this discrepancy is that water usually contains nanometer-sized cavitation nuclei. When the pressure decreases, these nuclei expand and become visible to the naked eye. However, the origin of these cavitation nuclei is not well understood. An earlier work in this field has mainly focused on the inception of nuclei which are purely composed of water vapor, whereas experimental data suggest that these nuclei are mainly composed of air. In this Letter, we develop a theoretical approach to study the inception of cavitation nuclei in water with uniformly dissolved air, using a diffuse interface approach. We derive equations which govern the transition of water with uniformly dissolved air to a critical state. Our results show that the dissolved air decreases the free energy barrier from the initial to the critical state, thereby aiding the formation of cavitation nuclei. This study opens up possibilities to explore cavitation inception in fluids containing dissolved gases.

Published under an exclusive license by AIP Publishing. https://doi.org/10.1063/5.0131165

I. INTRODUCTION

Cavitation is the formation of small vapor-filled bubbles in a liquid due to local depressurization. These bubbles are ubiquitous and play an important role in diverse phenomena such as soil erosion, swift movements of the fern sporangia, and accelerated food production.3 While the growth and collapse dynamics of these bubbles are well characterized, 4.5 the extent of depressurization required for their formation remains controversial.^{6,7} Although different theoretical estimates yield different values for the depressurization required to observe vapor bubbles at room temperature (300 K), ranging from -200 MPa using estimates based on molecular dynamics simulations⁸ to -120 MPa using the modified IAPWS-95 equation of state for water, it is generally accepted that cavitation pressure is much less than -25 MPa. However, experimentally we observe vapor-filled bubbles at much higher pressures (\approx 3 kPa at room temperature). The widely prevalent explanation is that liquids contain microscopic cavities that are filled with non-condensable gases (NCGs), also referred to as cavitation nuclei. These nuclei are nanometer sized and can persist in the liquid for time intervals of the order of 100 h. 10 When the pressure drops below a threshold pressure, which is commonly taken as the vapor pressure of the liquid (p_v) , these nuclei expand and become visible to the naked eye. While the presence of these nuclei can explain the lower depressurization required to generate bubbles which can be seen with the naked eye, the inception of these nuclei remains an open problem.

Classically, the inception of vapor nuclei in pure liquids has been studied using the nucleation theory. 11 When the pressure in a liquid decreases, a cloud of vapor-filled nuclei is formed. However, the nucleation rate (number of vapor nuclei formed per unit time per unit volume) is very small at high pressures. For instance, at a temperature of $50\,^{\circ}$ C and a pressure of $-70\,\mathrm{MPa}$, it would take $30\,\times\,10^9$ years to observe a single water vapor nucleus in a volume corresponding to the total volume of the earth's oceans. 12 Therefore, cavitation pressure (p_{cav}) is defined as the ambient pressure at which the rate of nucleation (J) of at least one vapor-filled nucleus in a volume V_{τ} within a time interval $0 \le t \le \tau$ is sufficiently large (of the order of 10^{10} or higher). Using this theory, the cavitation pressure of pure water at room temperature was estimated to be of the order of $-120 \,\mathrm{MPa}$, a value that has been validated with experiments on pure water found as quartz

When a liquid is depressurized, we observe a local reduction in the density of the liquid. However, this system, which consists of a region of smaller density surrounded by liquid with higher density, is not in thermodynamic equilibrium. While transitioning from this

depressurized liquid state to the thermodynamically stable state, where we have a vaporous nucleus in a pool of depressurized liquid, the fluid has to pass through a critical state where we have a critical nucleus in depressurized liquid. Transitioning to this critical state poses a free energy barrier, in which the system needs to overcome. The critical nucleation rate (J^*) strongly depends on this critical free energy barrier $(\Delta\Omega^*)$. Therefore, $\Delta\Omega^*$ must be evaluated accurately to predict the critical nucleation rate, which in turn determines the cavitation pressure. The earliest efforts to determine $\Delta\Omega^*$ were based on classical nucleation theory (CNT). This theory assumes a state of uniform pressure inside the nucleus up to the surface which divides the nucleus from the surrounding liquid. An interface of zero thickness separates the liquid and the nucleus, and surface tension (σ^*) is used to determine the critical free energy barrier through the formula $\Delta\Omega^* = 16\pi\sigma^{*3}/(3\Delta p^2)$, where Δp is the pressure difference between the interior of the nucleus and the surrounding liquid. 15 While this model can successfully predict the free energy barrier for the inception of large vaporous nuclei, it overestimates its value for smaller nuclei where the thickness of the dividing interface is of the order of the radius of the nuclei. Therefore, an additional parameter called the Tolman length was introduced to improve the prediction of CNT for small nuclei. An alternative approach to estimate $\Delta\Omega^*$ is based on diffuse interface (DI) models, which naturally account for the thickness of the liquid-nucleus interface.¹⁷ These methods rely on an Equation of State (EoS) to describe the properties of the fluid, which can be derived from a free energy per unit volume of the fluid (W). 18,19 DI models based on the IAPWS-95 EoS have been used to theoretically estimate p_{cav} for pure water as observed in experiments.¹²

However, these theories consider the formation of pure vapor nuclei in pure liquid water, whereas cavitation nuclei in water are primarily composed of air, 10 which is a NCG primarily composed of nitrogen. Recent experimental evidence also suggests that local NCG supersaturation is responsible for the nucleation of cavitation bubbles.²⁰ Therefore, accounting for the effect of NCGs in theoretical studies is imperative to bridge the gap between experiments and theory with respect to inception of cavitation nuclei. NCGs in liquids exist either in uniformly dissolved form or in the form of nanometer-sized nuclei. In this paper, we develop a theoretical framework to study inception of NCG-vapor nuclei in a pool of liquid with uniformly dissolved NCG. We develop a theoretical approach based on the diffuse interface (DI) theory to describe the properties of a fluid-NCG mixture, thereby taking into account the finite thickness of the interfaces separating liquid-vapor and liquid-NCG and generalizing the predictions from classical nucleation theory (CNT).

II. MODEL DEVELOPMENT AND VALIDATION

In this section, we describe our model for two-phase flows containing dissolved NCG. We also present validation cases for our model and derive relationships to relate physical properties in the DI and sharp interface descriptions of fluids. Throughout the paper, we have used the properties of nitrogen to understand the behavior of air as it is the predominant component. The superscripts a and w have been used to represent the properties of air and water, respectively, unless stated otherwise. The mass fraction (c) of air in an air—water mixture is

$$c = \frac{m^a}{m^a + m^w},\tag{1}$$

where m^a and m^w represent the mass of air and water, respectively. The mole fraction of air (x) can be represented as

$$x = \frac{m^a/M^a}{m^a/M^a + m^w/M^w},$$
 (2)

where M^a and M^w are the molar masses of air and water, respectively. The mole fraction and mass fraction of NCG in the mixture are related as

$$x = \frac{c}{c + \frac{M^a}{M^w}(1 - c)}.$$
 (3)

The molar mass of the mixture (*M*) can be written as

$$M = xM^a + (1 - x)M^w. (4)$$

A. Free energy of the mixture

We propose an expression for the free energy per unit volume (ψ) to describe the properties of a mixture of water and NCG as follows:

$$\psi = W(\rho, c, \theta) + \frac{\lambda(\theta)}{2} |\nabla \rho|^2 + \frac{\varepsilon^2(\theta)}{2} |\nabla c|^2.$$
 (5)

Here, c is the mass fraction of NCG, ρ is the density of the mixture, and θ is the temperature of the mixture. The temperature-dependent positive parameters $\lambda(\theta)$ and $\varepsilon^2(\theta)$ account for interfacial energies and are responsible for surface tension at the liquid–vapor and liquid–NCG interfaces, respectively. The function $W(\rho,c,\theta)$ describes the free energy per unit volume of the mixture in the regions away from the interfaces. It is based on the Peng–Robinson EoS²¹ and ideal mixing rules and can naturally account for phase transitions from liquid phase to vapor phase and vice versa. Mathematically,

$$W = R\theta \rho \ln \left(\frac{\rho}{b - \rho} \right) - \frac{ab\rho}{2\sqrt{2}} \ln \left| \frac{\rho - b(1 - \sqrt{2})}{\rho - b(1 + \sqrt{2})} \right| + R\theta \rho \left\{ c \ln (c) + (1 - c) \ln (1 - c) \right\}, \tag{6}$$

where R(c) is the specific gas constant of the mixture; $a=a(\theta,c)$ and b=b(c) are EoS specific parameters that depend on the temperature, the properties of the constituent fluids, and the composition of the mixture. Let us consider the specific case of an air–water mixture. Then, we have five parameters: R, a^w , and b^w are the parameters for water; whereas a^a and b^a are the parameters for air. The specific gas constant of the mixture can be written as

$$R = \frac{R_u}{M},\tag{7}$$

where $R_u = 8314 \text{ J mol}^{-1} \text{ K}^{-1}$ is the universal gas constant. The specific gas constants for water and air are equal to $R^w = 461.6$ and $R^a = 296.8 \text{ J kg}^{-1} \text{ K}^{-1}$, respectively. The parameters b^w and b^a are constants and depend on the critical properties of water and air, respectively, and have the following functional dependence:

$$b^{w,a} = 12.8538 \frac{p_c^{w,a}}{R^{w,a} \theta_c^{w,a}}, \tag{8}$$

where $\theta_c^{w,a}$ and $p_c^{w,a}$ are the critical temperature and critical pressure of water and air, respectively, whose values are given in Table I. Using these pure substance values, the parameter b for the mixture can be determined as follows:

$$b = \frac{b^{w}b^{a}}{xb^{w} + (1-x)b^{a}}. (9)$$

The parameters a^w and a^a also depend on the temperature of the mixture in addition to the critical properties of the constituent fluid, and this relationship can be expressed in the functional form as

$$a^{w,a} = a_c^{w,a} \alpha^{w,a}(\theta), \tag{10}$$

where the constants $a_c^{\rm w}$ and $a_c^{\rm a}$ can be expressed in terms of the critical properties of the respective fluid as

$$a_c^{w,a} = 0.457235 \frac{\left(R^{w,a}\theta_c^{w,a}\right)^2}{p_c^{w,a}}.$$
 (11)

The function $\alpha^w(\theta)$ is taken from the work of Li *et al.*²² It has the following functional form:

$$\alpha^{w}(\theta) = \left[w_1 + w_2 \left\{ 1 - \frac{\theta}{\theta_c^{w}} \right\} - w_3 \left\{ 1 - \left(\frac{\theta}{\theta_c^{w}} \right)^{-1} \right\} + w_4 \left\{ 1 - \left(\frac{\theta}{\theta_c^{w}} \right)^{-2} \right\} \right]^2, \tag{12}$$

where $w_1 = 1.00095$, $w_2 = 0.39222$, $w_3 = 0.07294$, and $w_4 = 0.00706$ are constants. The function $\alpha^a(\theta)$ is also taken from Li *et al.*²² and has the following form:

$$\alpha^{a}(\theta) = \exp\left[\left(a_{1} - a_{2}\omega^{a} + a_{3}\omega^{a2}\right)\left(1 - \frac{\theta}{\theta_{c}^{a}}\right) + a_{4}\ln\left\{1 + \left(a_{5} + a_{6}\omega^{a} - a_{7}\omega^{a2}\right)\left(1 - \sqrt{\frac{\theta}{\theta_{c}^{a}}}\right)\right\}\right], \quad (13)$$

where $a_1 = 0.132\,80$, $a_2 = 0.050\,52$, $a_3 = 0.259\,48$, $a_4 = 0.817\,69$, $a_5 = 0.313\,55$, $a_6 = 1.867\,45$, and $a_7 = 0.526\,04$ are constants. The constant ω^a is the acentric factor of air whose value is tabulated in Table I. The parameter a for the mixture can be determined as follows:

$$a = x^{2}a^{a} + (1 - x)^{2}a^{w} + 2x(1 - x)\sqrt{a^{a}a^{w}}(1 - \delta^{aw}), \tag{14}$$

where δ^{aw} is the binary interaction parameter between air and water. Its value varies with temperature as follows:²³

$$\delta^{aw}(\theta) = -1.70235 + 0.44338 \frac{\theta}{\theta_c^a}.$$
 (15)

B. Validation

As we are investigating the effect of uniformly dissolved air on the cavitation pressure of water, the EoS should accurately predict the solubility of air in water and the total pressure of the mixture. We compare the predictions of the above EoS to experimental results on solubility of air in liquid water and saturation vapor pressure of pure water, respectively.

1. Solubility of NCG in liquid

In this section, we will describe the general procedure of finding the phase equilibrium solutions; i.e., the equilibrium density and NCG concentration in the liquid state (ρ_l and c_b respectively) and the vapor state (ρ_v and c_v , respectively). Before proceeding further, we define the chemical potential of a species (μ) in a mixture as the rate of change of free energy of a thermodynamic system with respect to the change in the number of molecules of the species that are added to the system. Chemical potential is used to define the conditions for phase equilibrium of a binary mixture 24 at constant temperature using the following conditions:

$$\mu_{\nu}^{a} = \mu_{l}^{a}, \quad \mu_{\nu}^{w} = \mu_{l}^{w}, \quad p_{\nu} = p_{l},$$
 (16)

where the subscripts ν and l represent the vapor and liquid phases, respectively. Now, we determine expressions for chemical potential of water and air, respectively, using the definition from above. Let us consider a system with volume V_T , which contains N^a being the air molecules and N^w being the water molecules. Then, the density of the mixture and mass fraction of air can be written as

$$\rho = \frac{N^a M^a + N^w M^w}{V_T}, \quad c = \frac{N^a M^a}{N^a M^a + N^w M^w}. \tag{17}$$

From the definition of chemical potential of a component in a mixture,

$$\mu^{a} = \left[\frac{\partial(V_{T}W)}{\partial N^{a}}\right]_{\theta, V_{T}, N^{w}}, \quad \mu^{w} = \left[\frac{\partial(V_{T}W)}{\partial N^{w}}\right]_{\theta, V_{T}, N^{a}}.$$
 (18)

Writing the chemical potentials in terms of ρ and c, we get

$$\mu^{a} = V_{T} \left[\frac{\partial W}{\partial \rho} \frac{\partial \rho}{\partial N^{a}} + \frac{\partial W}{\partial c} \frac{\partial c}{\partial N^{a}} \right]_{\theta, V_{T}, N^{w}},$$

$$\mu^{w} = V_{T} \left[\frac{\partial W}{\partial \rho} \frac{\partial \rho}{\partial N^{w}} + \frac{\partial W}{\partial c} \frac{\partial c}{\partial N^{w}} \right]_{\theta, V_{T}, N^{a}}.$$
(19)

Taking the partial derivative of Eq. (17) with respect to N^a and N^w , we get

TABLE I. Physical and critical properties of nitrogen and water and their corresponding symbols in the manuscript.

Substance	Molar mass (g mol ⁻¹)	Critical temperature (K)	Critical pressure (MPa)	Acentric factor
Air	$14.0067 (M^a)$	126.03 (θ_c^a)	3.395 (p_c^a)	0.039 (ω^a)
Water	$18.0152 (M^w)$	647.10 (θ_c^w)	22.064 (p_c^w)	0.344 (ω^w)

$$\frac{\partial \rho}{\partial N^{a}} = \frac{M^{a}}{V_{T}}, \quad \frac{\partial \rho}{\partial N^{w}} = \frac{M^{w}}{V_{T}},$$

$$\frac{\partial c}{\partial N^{a}} = \frac{N^{w}M^{a}M^{w}}{\left(N^{a}M^{a} + N^{w}M^{w}\right)^{2}}, \quad \frac{\partial c}{\partial N^{w}} = -\frac{N^{a}M^{a}M^{w}}{\left(N^{a}M^{a} + N^{w}M^{w}\right)^{2}}.$$
(20)

Substituting the expressions from Eq. (20) into Eq. (19) and simplifying, we get

$$\frac{\mu^{a}}{M^{a}} = \left[\frac{\partial W}{\partial \rho} + \frac{(1-c)}{\rho} \frac{\partial W}{\partial c} \right], \quad \frac{\mu^{w}}{M^{w}} = \left[\frac{\partial W}{\partial \rho} - \frac{c}{\rho} \frac{\partial W}{\partial c} \right]. \tag{21}$$

These are the required expressions for the chemical potential of air and water in an air–water mixture. These are required in addition to the pressure to get the phase equilibrium conditions. The pressure in defined directly from the Helmholtz free energy per unit volume as follows:

$$p = \rho \frac{\partial W}{\partial \rho} - W. \tag{22}$$

Therefore, for a given ambient pressure p_a , the four equations required to determine $\rho_b \rho_v$, c_b and c_v are as follows:

$$\frac{\partial W}{\partial \rho} (\rho_{\nu}, c_{\nu}) + \frac{(1 - c_{\nu})}{\rho_{\nu}} \frac{\partial W}{\partial c} (\rho_{\nu}, c_{\nu})$$

$$= \frac{\partial W}{\partial \rho} (\rho_{l}, c_{l}) + \frac{(1 - c_{l})}{\rho_{l}} \frac{\partial W}{\partial c} (\rho_{l}, c_{l}), \qquad (23a)$$

$$\frac{\partial W}{\partial \rho} (\rho_{\nu}, c_{\nu}) - \frac{c_{\nu}}{\rho_{\nu}} \frac{\partial W}{\partial c} (\rho_{\nu}, c_{\nu})$$

$$= \frac{\partial W}{\partial \rho} (\rho_{l}, c_{l}) - \frac{c_{l}}{\rho_{l}} \frac{\partial W}{\partial c} (\rho_{l}, c_{l}), \qquad (23b)$$

$$p_{a} = \rho_{l} \frac{\partial W}{\partial \rho} (\rho_{l}, c_{l}) - W(\rho_{l}, c_{l}), \tag{23c}$$

$$p_{a} = \rho_{\nu} \frac{\partial W}{\partial \rho} (\rho_{\nu}, c_{\nu}) - W(\rho_{\nu}, c_{\nu}). \tag{23d}$$

We repeat this procedure for different values of θ to get the equilibrium concentration of air in liquid water (c_l) for different ambient pressures (p_a) and plot in Fig. 1. Our model predictions show excellent agreement with experimental results.

2. Saturation vapor pressure of water

In this section, we will describe the procedure to calculate the saturation vapor pressure of pure water from mixture the free energy in Eq. (6). Here, c=0, and the free energy of the fluid per unit volume from Eq. (6) reduces to

$$W = R^{w}\theta\rho \ln\left(\frac{\rho}{b^{w} - \rho}\right) - \frac{a^{w}b^{w}\rho}{2\sqrt{2}}\ln\left|\frac{\rho - b^{w}(1 - \sqrt{2})}{\rho - b^{w}(1 + \sqrt{2})}\right|. \tag{24}$$

Here, we wish to obtain the equilibrium densities ρ_l^w and ρ_v^w in the liquid and vapor phases, respectively, corresponding to a given temperature θ . Similar to Eq. (16), our equilibrium conditions are derived from the equality of chemical potential and pressure of both phases. Substituting the expressions developed in Sec. II B 1 and simplifying, we obtain the required set of two equations that can be solved to obtain ρ_l^w and ρ_v^w . These are as follows:

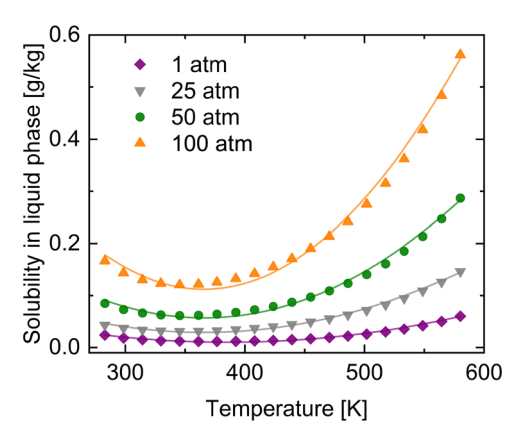


FIG. 1. Comparison of solubility of nitrogen in liquid water obtained using the EoS from Eq. (6) with experimental results for $\theta \in [280, 580]$ K for ambient pressures of 1, 25, 50, and 100 atm. The dots show experimental results, whereas the solid lines show predictions from the EoS.

$$\frac{\partial W}{\partial \rho} \left(\rho_l^w \right) = \frac{\partial W}{\partial \rho} \left(\rho_v^w \right),$$

$$\rho_l^w \frac{\partial W}{\partial \rho} \left(\rho_l^w \right) - W(\rho_l^w) = \rho_v^w \frac{\partial W}{\partial \rho} \left(\rho_v^w \right) - W(\rho_v^w).$$
(25)

After solving Eq. (25), we obtain ρ_{ν} , from which we can obtain the saturation vapor pressure as the pressure corresponding to that density value using the following formula:

$$p_{sat} = \rho_{\nu}^{w} \frac{\partial W}{\partial \rho} \left(\rho_{\nu}^{w} \right) - W(\rho_{\nu}^{w}). \tag{26}$$

We repeat this procedure for different values of θ to obtain the saturation vapor pressure curve as shown in Fig. 2. Again, we see excellent agreement with experimental results.

C. Equations to relate physical properties in the DI and sharp-interface models

In this paper, we are studying the problem of nucleation of a single NCG-vapor nucleus in a pool of liquid using the diffuse interface

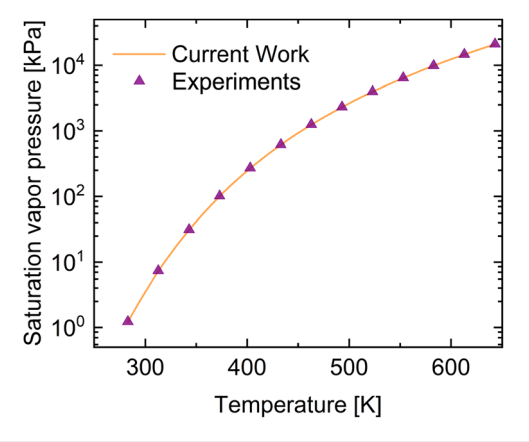


FIG. 2. Comparison of saturation vapor pressure for pure water obtained using the EoS from Eq. (6) with experimental results 26 for $\theta \in [277,647]$ K.

(DI) approach. We are interested in the equilibrium transformation of a fluid with uniform density ρ_l^s , with uniformly dissolved NCG c_l^s , into a spherical bubble with density ρ_s^s and concentration of dissolved NCG c_s^s at the center (r=0) which is surrounded by liquid with uniform density ρ_l^s and uniformly dissolved NCG c_s^s . As both of these are equilibrium configurations, they can be obtained by minimizing the free energy functional

$$J_{L} = \int_{\Omega} \left(W + \frac{\lambda}{2} |\nabla \rho|^{2} + \frac{\varepsilon^{2}}{2} |\nabla c|^{2} - L_{1}\rho - L_{2}\rho c \right) d\Omega, \qquad (27)$$

where Ω is our domain of interest, and L_1 and L_2 are constant Lagrange multipliers to enforce the conservation of total mass and conservation of mass of NCG, respectively. The Euler–Lagrange equations associated with the minimization of J_L are as follows:

$$\frac{\partial W}{\partial \rho} - \lambda \Delta \rho - L_1 - L_2 c = 0, \tag{28a}$$

$$\frac{\partial W}{\partial c} - \varepsilon^2 \Delta c - L_2 \rho = 0. \tag{28b}$$

As we are interested in obtaining the density and concentration profile of a spherical bubble, we express Eqs. (28a) and (28b) in spherical coordinates

$$\frac{\partial W}{\partial \rho} = \lambda \left(\rho_{,rr} + \frac{2}{r} \rho_{,r} \right) + L_1 + L_2 c, \tag{29a}$$

$$\frac{\partial W}{\partial c} = \varepsilon^2 \left(c_{,rr} + \frac{2}{r} c_{,r} \right) + L_2 \rho. \tag{29b}$$

Here, () $_{,r}$ represents the derivative along the radial direction. Multiplying Eq. (29a) by $\rho_{,r}$ and Eq. (29b) by $c_{,r}$ and adding

$$\frac{\partial W}{\partial \rho} \rho_{,r} + \frac{\partial W}{\partial c} c_{,r} = \lambda \left(\rho_{,rr} + \frac{2}{r} \rho_{,r} \right) \rho_{,r} + \varepsilon^2 \left(c_{,rr} + \frac{2}{r} c_{,r} \right) c_{,r} + L_1 \rho_{,r} + L_2 (c \rho_{,r} + \rho c_{,r}), \tag{30}$$

which can be further simplified as

$$W_{,r} = \frac{\lambda}{2} \left(\rho_{,r}^2 \right)_{,r} + \frac{2\lambda}{r} \rho_{,r}^2 + \frac{\varepsilon^2}{2} \left(c_{,r}^2 \right)_{,r} + \frac{2\varepsilon}{r} c_{,r}^2 + L_1 \rho_{,r} + L_2 (\rho c)_{,r}.$$
(31)

Integrating between the limits 0 to r, we get

$$W(\rho, c) - W(\rho_{\nu}^{s}, c_{\nu}^{s}) = \frac{\lambda}{2} \rho_{,r}^{2} + 2\lambda \int_{0}^{r} \frac{1}{r} \rho_{,r}^{2} dr + \frac{\varepsilon^{2}}{2} c_{,r}^{2}$$

$$+2\varepsilon^{2} \int_{0}^{r} \frac{1}{r} c_{,r}^{2} dr + L_{1}(\rho - \rho_{\nu}^{s}) + L_{2}(\rho c - \rho_{\nu}^{s} c_{\nu}^{s}).$$
(32)

Multiplying both sides of Eq. (32) by $r^3/3$ and evaluating the resulting expression as $r \to \infty$, we get

$$\lim_{r \to \infty} \left[\frac{r^{3}}{3} \left\{ W(\rho_{l}^{s}, c_{l}^{s}) - W(\rho_{v}^{s}, c_{v}^{s}) - L_{1}(\rho_{l}^{s} - \rho_{v}^{s}) - L_{2}(\rho_{l}^{s} c_{l}^{s} - \rho_{v}^{s} c_{v}^{s}) \right\} \right] = \lim_{r \to \infty} \left[\frac{2}{3} \lambda r^{3} \int_{0}^{r} \frac{1}{r} \rho_{,r}^{2} dr + \frac{2}{3} \varepsilon^{2} r^{3} \int_{0}^{r} \frac{1}{r} c_{,r}^{2} dr \right].$$
(33)

Multiplying both sides of Eq. (32) by r^2 and integrating from 0 to ∞ , we get

$$\int_{0}^{\infty} \{W(\rho,c) - W(\rho_{v}^{s},c_{v}^{s}) - L_{1}(\rho - \rho_{v}^{s}) - L_{2}(\rho c - \rho_{v}^{s}c_{v}^{s})\}r^{2}dr$$

$$= \frac{\lambda}{2} \int_{0}^{\infty} r^{2} \rho_{,r}^{2} dr + \frac{\varepsilon^{2}}{2} \int_{0}^{\infty} r^{2} c_{,r}^{2} dr + 2\lambda \int_{0}^{\infty} r^{2} \left(\int_{0}^{r} \frac{1}{z} \rho_{,z}^{2} dz\right) dr$$

$$+2\varepsilon^{2} \int_{0}^{\infty} r^{2} \left(\int_{0}^{r} \frac{1}{z} c_{,z}^{2} dz\right) dr. \tag{34}$$

Rearranging terms on the left hand side of Eq. (34) and integrating the terms on right hand side by parts, we get

$$\int_{0}^{\infty} \left\{ W(\rho, c) - W(\rho_{l}^{s}, c_{l}^{s}) - L_{1}(\rho - \rho_{l}^{s}) - L_{2}(\rho c - \rho_{l}^{s} c_{l}^{s}) \right\} r^{2} dr + \int_{0}^{\infty} \left\{ W(\rho_{l}^{s}, c_{l}^{s}) - W(\rho_{v}^{s}, c_{v}^{s}) - L_{2}(\rho_{l}^{s} c_{l}^{s} - \rho_{v}^{s} c_{v}^{s}) \right\} r^{2} dr \\
= \frac{\lambda}{2} \int_{0}^{\infty} r^{2} \rho_{,r}^{2} dr + \frac{\varepsilon^{2}}{2} \int_{0}^{\infty} r^{2} c_{,r}^{2} dr - 2\lambda \int_{0}^{\infty} \frac{1}{3} r^{2} \rho_{,r}^{2} dr \\
-2\varepsilon^{2} \int_{0}^{\infty} \frac{1}{3} r^{2} c_{,r}^{2} dr + \lim_{r \to \infty} \left\{ \frac{2\lambda}{3} r^{3} \int_{0}^{r} \frac{1}{z} \rho_{,z}^{2} dz + \frac{2\varepsilon^{2}}{3} r^{3} \int_{0}^{r} \frac{1}{z} c_{,z}^{2} dz \right\} \\
- \left\{ \frac{2\lambda}{3} r^{3} \int_{0}^{r} \frac{1}{z} \rho_{,z}^{2} dz + \frac{2\varepsilon^{2}}{3} r^{3} \int_{0}^{r} \frac{1}{z} c_{,z}^{2} dz \right\}_{r=0}. \tag{35}$$

Using Eq. (33), we can write

$$\int_{0}^{\infty} \left\{ W(\rho, c) - W(\rho_{l}^{s}, c_{l}^{s}) - L_{1}(\rho - \rho_{l}^{s}) - L_{2}(\rho c - \rho_{l}^{s} c_{l}^{s}) \right\} r^{2} dr + \int_{0}^{\infty} \left\{ W(\rho_{l}^{s}, c_{l}^{s}) - W(\rho_{v}^{s}, c_{v}^{s}) - L_{2}(\rho_{l}^{s} c_{l}^{s} - \rho_{v}^{s} c_{v}^{s}) \right\} r^{2} dr \\
= \frac{\lambda}{2} \int_{0}^{\infty} r^{2} \rho_{,r}^{2} dr + \frac{\varepsilon^{2}}{2} \int_{0}^{\infty} r^{2} c_{,r}^{2} dr - 2\lambda \int_{0}^{\infty} \frac{1}{3} r^{2} \rho_{,r}^{2} dr \\
-2\varepsilon^{2} \int_{0}^{\infty} \frac{1}{3} r^{2} c_{,r}^{2} dr + \lim_{r \to \infty} \left[\frac{r^{3}}{3} \left\{ W(\rho_{l}^{s}, c_{l}^{s}) - W(\rho_{v}^{s}, c_{v}^{s}) - L_{2}(\rho_{l}^{s} c_{l}^{s} - \rho_{v}^{s} c_{v}^{s}) \right\} \right]. \tag{36}$$

Simplifying Eq. (36) further, we get

$$\int_{0}^{\infty} \left\{ W(\rho, c) - W(\rho_{l}^{s}, c_{l}^{s}) - L_{1}(\rho - \rho_{l}^{s}) - L_{2}(\rho c - \rho_{l}^{s} c_{l}^{s}) + \frac{\lambda}{2} \rho_{,r}^{2} + \frac{\varepsilon^{2}}{2} c_{,r}^{2} \right\} r^{2} dr$$

$$= \frac{\lambda}{3} \int_{0}^{\infty} r^{2} \rho_{,r}^{2} dr + \frac{\varepsilon^{2}}{3} \int_{0}^{\infty} r^{2} c_{,r}^{2} dr.$$
(37)

Multiplying both sides of Eq. (37) by 4π , we get

$$4\pi \int_{0}^{\infty} \left\{ W(\rho, c) - W(\rho_{l}^{s}, c_{l}^{s}) - L_{1}(\rho - \rho_{l}^{s}) - L_{2}(\rho c - \rho_{l}^{s} c_{l}^{s}) + \frac{\lambda}{2} \rho_{,r}^{2} + \frac{\varepsilon^{2}}{2} c_{,r}^{2} \right\} r^{2} dr$$

$$= \frac{4}{3} \pi \int_{0}^{\infty} \{ \lambda \rho_{,r}^{2} + \varepsilon^{2} c_{,r}^{2} \} r^{2} dr.$$
(38)

Here, the integral on the left hand side is the excess free energy when we have a NCG–vapor bubble surrounded by liquid as compared to the case where we only have liquid. On the right hand side of the equation, we have a third of the energy required to create the interface between the two phases. Therefore, Eq. (38) indicates that the excess free energy required to create a NCG–vapor bubble in a pool of liquid is equal to one-third of the energy required to create the liquid–vapor interface. This result is consistent with results from sharp-interface theories. Now, our objective is to find equivalent expressions for the bubble radius (R), the excess pressure in the interior of the bubble (Δp), the excess free energy ($\Delta \Omega$), and surface tension (σ) for the DI model. Classically, they are related using the following relationships:

$$\Delta p = \frac{2\sigma}{R}, \ \Delta \Omega = \frac{4}{3}\pi R^2 \sigma,$$
 (39)

where we have already shown that for DI models

$$\Delta\Omega = \frac{4}{3}\pi \int_0^\infty \left(\lambda \rho_{,r}^2 + \varepsilon^2 c_{,r}^2\right) r^2 dr. \tag{40}$$

Here, we invoke the concept of nonlocal pressure (p^{nl}) , which is a true indicator of the pressure in DI models. The thermodynamic pressure, as defined in Eq. (22), is non-monotonic along the radial direction for an equilibrium solution (spherical NCG–vapor bubble in a pool of liquid), whereas the nonlocal pressure remains monotonic for an equilibrium solution in a DI model. It is related to the thermodynamic pressure as follows:

$$p^{nl}(\rho, c, \nabla \rho, \nabla c) = p(\rho, c) + \frac{\lambda}{2} |\nabla \rho|^2 - \lambda \rho \Delta \rho + \frac{\varepsilon^2}{2} |\nabla c|^2.$$
 (41)

At r=0, we have nucleation of a vapor bubble, so we have $\rho=\rho_{\nu}^{s}$. Furthermore, from symmetry, it follows that $\rho_{,r}=0$, $c_{,r}=0$. Therefore, we use Eq. (28a) to calculate the nonlocal pressure inside the bubble (p_{ν}^{nl})

$$p_{\nu}^{nl} = \left\{ \rho \frac{\partial W}{\partial \rho} - W - \lambda \rho \Delta \rho \right\}_{(\rho_{\nu}^{s}, c_{\nu}^{s})} = -W(\rho_{\nu}^{s}, c_{\nu}^{s}) + L_{1}\rho_{\nu}^{s} + L_{2}\rho_{\nu}^{s}c_{\nu}^{s}.$$

$$(42)$$

Away from the bubble, we have $\rho = \rho_l^s$, $\rho_{,r} = 0$, $c_{,r} = 0$. Therefore, the nonlocal pressure sufficiently away from the bubble (p_l^{nl}) can be written as

$$p_l^{nl} = \left\{ \rho \frac{\partial W}{\partial \rho} - W - \lambda \rho \Delta \rho \right\}_{\left(\rho_l^s, c_l^s\right)} = -W(\rho_l^s, c_l^s) + L_1 \rho_l^s + L_2 \rho_l^s c_l^s.$$
(43)

Therefore, the difference in pressure (Δp) can be written as

$$\Delta p = p_{\nu}^{nl} - p_{l}^{nl} = W(\rho_{l}^{s}, c_{l}^{s}) - W(\rho_{\nu}^{s}, c_{\nu}^{s}) + L_{1}(\rho_{\nu}^{s} - \rho_{l}^{s}) + L_{2}(\rho_{\nu}^{s} c_{\nu}^{s} - \rho_{l}^{s} c_{l}^{s}).$$
(44)

Comparing the DI expressions from Eqs. (44) and (40) to the corresponding sharp interface classical expressions from Eq. (39), we get

$$R = \left[2 \int_{0}^{\infty} \left(\lambda \rho_{,r}^{2} + \varepsilon^{2} c_{,r}^{2} \right) r^{2} dr \right]^{\frac{1}{3}} \left[W(\rho_{l}^{s}, c_{l}^{s}) - W(\rho_{v}^{s}, c_{v}^{s}) + L_{1}(\rho_{v}^{s} - \rho_{l}^{s}) + L_{2}(\rho_{v}^{s} c_{v}^{s} - \rho_{l}^{s} c_{l}^{s}) \right]^{-\frac{1}{3}},$$

$$\sigma = \left[\frac{1}{4} \int_{0}^{\infty} \left(\lambda \rho_{,r}^{2} + \varepsilon^{2} c_{,r}^{2} \right) r^{2} dr \right]^{\frac{1}{3}} \left[W(\rho_{l}^{s}, c_{l}^{s}) - W(\rho_{v}^{s}, c_{v}^{s}) + L_{1}(\rho_{v}^{s} - \rho_{l}^{s}) + L_{2}(\rho_{v}^{s} c_{v}^{s} - \rho_{l}^{s} c_{l}^{s}) \right]^{\frac{2}{3}},$$

$$\Delta \Omega = 4\pi \int_{0}^{\infty} \left\{ W(\rho, c) - W(\rho_{l}^{s}, c_{l}^{s}) - L_{1}(\rho - \rho_{l}^{s}) - L_{2}(\rho c - \rho_{l}^{s} c_{l}^{s}) + \frac{\lambda}{2} \rho_{,r}^{2} + \frac{\varepsilon^{2}}{2} c_{,r}^{2} \right\} r^{2} dr.$$

$$(45)$$

The set of relations proposed in Eq. (45) can be used to determine the radius of the bubble, the free energy excess and the surface tension for any equilibrium bubble with density and concentration profile $\rho(r)$ and c(r).

III. RESULTS

We employ the EoS to determine the cavitation pressure. We are interested in the inception of nuclei composed of a mixture of air and water in a pool of liquid water with uniformly dissolved air due to depressurization, for which we employ numerical simulations. Our initial condition is depressurized liquid water with uniform density ρ_L^* and uniformly dissolved NCG c_L^* , where the liquid pressure is given as $p_L^* = \rho_L^* \partial W/\partial \rho(\rho_L^*, c_L^*) - W(\rho_L^*, c_L^*)$. We are interested in the equilibrium transformation of this initial state to the critical state, where we have a spherical vapor–air nucleus in a pool of liquid water with uniformly dissolved air. This critical state also represents the state of maximum free energy, which must be surmounted before this thermodynamic system can transition into an equilibrium solution. From the Euler–Lagrange equations (29a) and (29b), we can write

$$\frac{\partial W}{\partial \rho} \left(\rho_L^*, c_L^* \right) = L_1^* + L_2^* c_L^*, \tag{46a}$$

$$\frac{\partial W}{\partial c} \left(\rho_L^*, c_L^* \right) = L_2^* \rho_L^*, \tag{46b}$$

where L_1^* and L_2^* are constant Lagrange multipliers to enforce the conservation of total mass and conservation of mass of NCG. Algebraic manipulation of Eqs. (46a) and (46b) gives

$$L_2^* = \frac{1}{a_L^*} \frac{\partial W}{\partial c} \left(\rho_L^*, c_L^* \right), \tag{47a}$$

$$L_{1}^{*} = \frac{\partial W}{\partial \rho} \left(\rho_{L}^{*}, c_{L}^{*} \right) - \frac{c_{L}^{*}}{\rho_{L}^{*}} \frac{\partial W}{\partial c} \left(\rho_{L}^{*}, c_{L}^{*} \right). \tag{47b}$$

We are interested in obtaining the critical (albeit unstable) configuration, which has the same chemical potential as the initial condition described above. To obtain this configuration, we solve the equations below to obtain the sequence of density and concentration configurations along the minimum energy path (MEP) from the initial state to the critical state²⁷

$$\frac{\partial \rho^{k}}{\partial \tilde{t}} = L_{1}^{*} - \left[\frac{\partial W}{\partial \rho} \left(\rho^{k}, c^{k} \right) - \frac{\lambda}{r^{2}} \left(r^{2} \rho_{,r}^{k} \right)_{,r} \right] \\
- \left[\frac{c^{k}}{\rho^{k}} \frac{\partial W}{\partial c} \left(\rho^{k}, c^{k} \right) + \frac{c^{k}}{\rho^{k}} \frac{\varepsilon^{2}}{r^{2}} \left(r^{2} c_{,r}^{k} \right)_{,r} \right], \qquad (48)$$

$$\frac{\partial c^{k}}{\partial \tilde{t}} = L_{2}^{*} - \left[\frac{1}{\rho_{k}} \frac{\partial W}{\partial c} \left(\rho^{k}, c^{k} \right) - \frac{1}{\rho^{k}} \frac{\varepsilon^{2}}{r^{2}} \left(r^{2} c_{,r}^{k} \right)_{,r} \right].$$

Here, $\rho^k(r,\tilde{t})$ and $c^k(r,\tilde{t})$ represent the density and NCG concentration configurations, respectively, and \tilde{t} is the pseudo time along the MEP; $L_2^* = 1/\rho_L^*\partial W/\partial c(\rho_L^*,c_L^*)$ and $L_1^* = \partial W/\partial \rho(\rho_L^*,c_L^*) - L_2^*c_L^*$ are the difference in chemical potential of NCG and water, and the chemical potential of water, respectively. We solve Eq. (48) using a centered second-order accurate finite difference scheme in space and the forward Euler scheme in time. For every solution (ρ^k,c^k) , we calculate the corresponding free energy barrier $[\Delta\Omega^k(\tilde{t})]$ using

$$\begin{split} \Delta\Omega^{k}(\tilde{t}) &= 4\pi \int_{0}^{\infty} \left\{ W(\rho^{k}, c^{k}) - W(\rho_{L}^{*}, c_{L}^{*}) \right\} r^{2} \mathrm{d}r \\ &- 4\pi \int_{0}^{\infty} \left\{ L_{1}(\rho^{k} - \rho_{L}^{*}) + L_{2}(\rho^{k} c^{k} - \rho_{L}^{*} c_{L}^{*}) \right\} r^{2} \mathrm{d}r \\ &+ 4\pi \int_{0}^{\infty} \left\{ \frac{\lambda}{2} \left(\rho_{,r}^{k} \right)^{2} + \frac{\varepsilon^{2}}{2} \left(c_{,r}^{k} \right)^{2} \right\} r^{2} \mathrm{d}r. \end{split} \tag{49}$$

Denoting $t^* = \operatorname{argmax}_{\tilde{t}} \Delta \Omega^k(\tilde{t})$, the critical nucleus profile is defined as $[\rho^c(r), c^c(r)] = [\rho^k(r, t^*), c^k(r, t^*)]$, and the critical free energy barrier is $\Delta \Omega^* = \Delta \Omega^k(t^*)$. We use the critical profile to obtain the surface tension of the critical nucleus and the pressure difference between the critical nucleus and the ambient liquid, which are used to calculate the critical nucleation rate using Eq. (45) as follows:

$$\sigma^{*} = \left[\frac{1}{4}\int_{0}^{\infty} \left\{ \lambda(\rho_{,r}^{c})^{2} + \varepsilon^{2}(c_{,r}^{c})^{2} \right\} r^{2} dr \right]^{\frac{1}{3}} \left[W(\rho_{L}^{*}, c_{L}^{*}) - W(\rho_{V}^{*}, c_{V}^{*}) + L_{1}^{*}(\rho_{V}^{*} - \rho_{L}^{*}) + L_{2}^{*}(\rho_{V}^{*} c_{V}^{*} - \rho_{L}^{*} c_{L}^{*}) \right]^{\frac{2}{3}},$$

$$\Delta p^{*} = \rho_{V}^{*} \frac{\partial W}{\partial \rho} (\rho_{V}^{*}, c_{V}^{*}) - W(\rho_{V}^{*}, c_{V}^{*}) - \rho_{L}^{*} \frac{\partial W}{\partial \rho} (\rho_{L}^{*}, c_{L}^{*}) + W(\rho_{L}^{*}, c_{L}^{*}),$$

$$J^{*} = \frac{\rho_{L}^{*} \rho_{V}^{*}}{M} \sqrt{\frac{k_{B} \theta(\sigma^{*})^{3}}{\eta \Delta p^{*}}} \exp\left\{-\Delta \Omega^{*} / (k_{B} \theta)\right\},$$
(50)

where M is the molar mass of the mixture, η is the viscosity of the mixture, and k_B is the Boltzmann constant. In Fig. 3, we plot J^* vs the ambient liquid pressure p_L^* . We observe that the rate of nucleation increases exponentially with a decrease in ambient pressure, which is consistent with DI calculations for pure water. 12 As the temperature increases, the rate of nucleation corresponding to a given p_I^* increases. Finally, as we increase the value of c_I^* at a given temperature, the nucleation rate increases. Cavitation occurs when the critical nucleation rate exceeds a threshold value. In this work, we choose a threshold value equal to 10¹⁰, which corresponds to the formation of 10¹⁰ nuclei in a volume of 1 mm³ every ns (cavitation pressure is not strongly affected by this choice¹² as the variation of nucleation rate with pressure is exponential). In Fig. 4, we plot the pressure corresponding to the threshold nucleation rate of 10¹⁰ vs temperature. There is a large scatter in experimental observations for cavitation pressure in pure water at small temperatures (<500 K), but the values converge at higher temperatures. Our approach can capture the experimental data correctly at higher temperatures. Dissolution of air in water increases the cavitation pressure, and the increase is higher at high temperatures. The difference in cavitation pressure between c = 0 and c = 0.01 is of the order of 1 MPa at room temperatures (yellow inset in Fig. 4) and increases to about 10 MPa at 580 K (green inset in Fig. 4). The difference produced due to uniformly dissolved air in liquid water is consistent with experimental observations for acoustically induced cavitation in liquid water containing dissolved oxygen and nitrogen, which is also shown in Fig. 4.

In conclusion, we propose a methodology to determine the cavitation pressure of liquids containing uniformly dissolved NCGs using the DI approach. We use an EoS based on the Peng–Robinson EoS and present validation cases to show that it can predict the saturation vapor pressure of pure water and solubility of air in liquid water over a large temperature range. The cavitation pressure plots show that dissolution of NCG increases the cavitation pressure. The difference is $\sim\!\!1$ MPa at room temperature and becomes $\sim\!\!10$ MPa as the temperature is increased to 600 K when we consider water with uniformly dissolved air with mass fraction c=0.01. Recent experiments show that locally accumulated NCG in liquids lowers the threshold for inception of cavitation nuclei due to a reduction in the strength of hydrogen bonds between water molecules and reduction of surface tension. 20 Our previous work also shows that NCG bubbles in liquids enhance the rate of

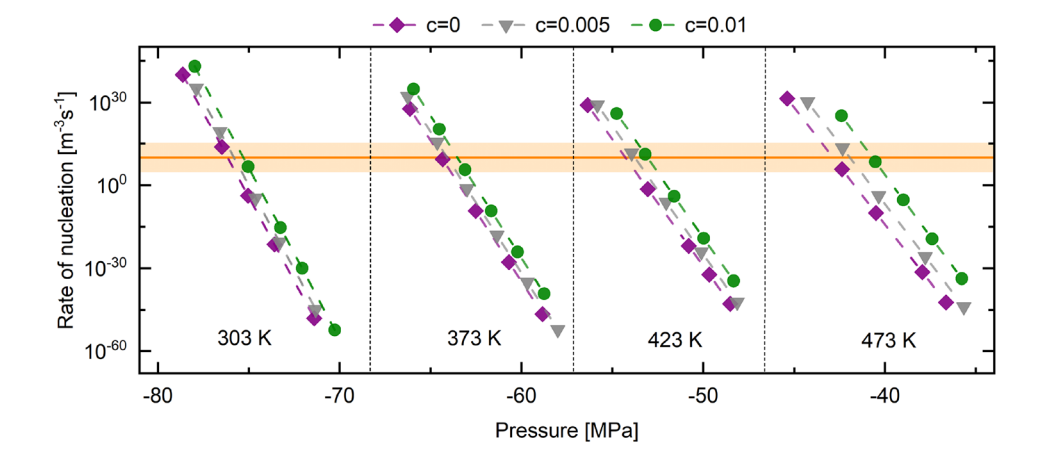


FIG. 3. Nucleation rate of critical bubble vs liquid pressure at $\theta=303,373,423$, and 473 K for different amounts of uniformly dissolved NCG (c_l^*) . The horizontal orange line represents the critical nucleation rate.

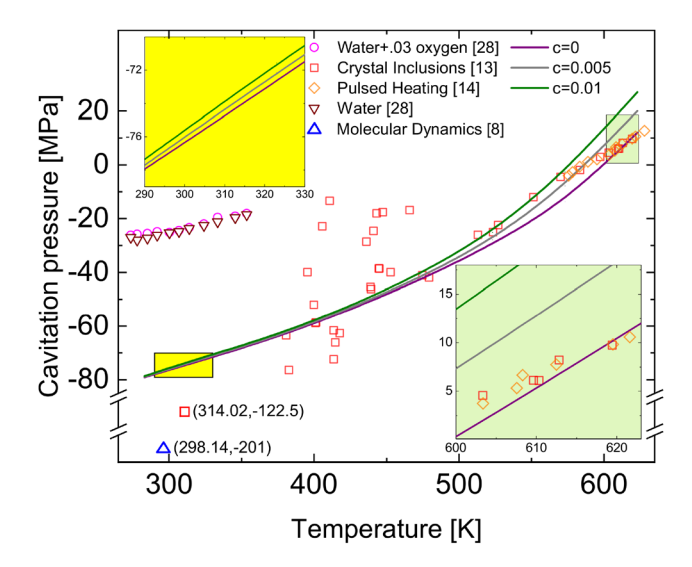


FIG. 4. Variation of cavitation pressure in the temperature range $\theta \in [280,630]$ K for different mass fractions of uniformly dissolved air in liquid water. The red squares correspond to the experimental observations for pure water found as quartz crystal inclusions, ¹³ whereas the orange rhombi represent data from experiments on pulsed heating of water. ¹⁴ The inverted brown triangles correspond acoustically induced cavitation experiments in pure water. ²⁸ The magenta circle shows acoustic cavitation experiments on pure water with dissolved oxygen, ²⁸ whereas the blue triangle represents the theoretical estimate at room temperature using molecular dynamics. ⁸

transformation of a fluid from liquid phase to vapor phase through a mass transfer mechanism primarily governed by diffusion of NCG.^{29,30} This work opens avenues to theoretically understand phenomena related to cavitation inception, such as the formation of additional cavitation bubbles when some cavitation bubbles are already present, from a thermodynamic perspective, in much more detail.

ACKNOWLEDGMENTS

The authors gratefully acknowledge the support from the U.S. Department of Defense under the DEPSCoR program (Award No. FA9550-20-1-0165) and the National Science Foundation (Award No. CBET 1805817). The opinions, findings, and conclusions or recommendations expressed are those of the authors and do not necessarily reflect the views of the funding agencies.

AUTHOR DECLARATIONS

Conflict of Interest

The authors have no conflicts to disclose.

Author Contributions

Saikat Mukherjee: Writing – original draft (equal). **Hector Gomez:** Supervision (equal).

DATA AVAILABILITY

The data that support the findings of this study are available from the corresponding author upon reasonable request.

REFERENCES

- ¹Y. Zhang, Z. Qian, B. Ji, and Y. Wu, "A review of microscopic interactions between cavitation bubbles and particles in silt-laden flow," Renewable Sustainable Energy Rev. 56, 303–318 (2016).
- ²M. Bruning, M. Costalonga, J. Snoeijer, and A. Marin, "Turning drops into bubbles: Cavitation by vapor diffusion through elastic networks," Phys. Rev. Lett. 123, 214501 (2019).
- ³S. Tursunbayeva, A. Iztayev, A. Mynbayeva, M. Alimardanova, B. Iztayev, and M. Yakiyayeva, "Development of a highly efficient ion-ozone cavitation technology for accelerated bread production," Sci. Rep. 11, 19129 (2021).
- ⁴M. S. Plesset and A. Prosperetti, "Bubble dynamics and cavitation," Annu. Rev. Fluid Mech. **9**, 145–185 (1977).
- ⁵L. van Wijngaarden, "Mechanics of collapsing cavitation bubbles," Ultrason. Sonochem. 29, 524–527 (2016).
- ⁶L. A. Crum, "Tensile strength of water," Nature 278, 148–149 (1979).
- ⁷E. Herbert, S. Balibar, and F. Caupin, "Cavitation pressure in water," Phys. Rev. E 74, 041603 (2006).
- ⁸Y. Zhou, B. Li, Y. Gu, and M. Chen, "A molecular dynamics simulation study on the cavitation inception of water with dissolved gases," Mol. Phys. 117, 1894–1902 (2019).
- ⁹G. Menzl, M. A. Gonzalez, P. Geiger, F. Caupin, J. L. Abascal, C. Valeriani, and C. Dellago, "Molecular mechanism for cavitation in water under tension," Proc. Natl. Acad. Sci. 113, 13582–13587 (2016).
- ¹⁰K. A. Mørch, "Cavitation inception from bubble nuclei," Interface Focus 5, 20150006 (2015).
- ¹¹A. Aasen, D. Reguera, and Ø. Wilhelmsen, "Curvature corrections remove the inconsistencies of binary classical nucleation theory," Phys. Rev. Lett. 124, 045701 (2020).
- ¹²F. Magaletti, M. Gallo, and C. M. Casciola, "Water cavitation from ambient to high temperatures," Sci. Rep. 11, 20801 (2021).
- ¹³Q. Zheng, D. Durben, G. Wolf, and C. Angell, "Liquids at large negative pressures: Water at the homogeneous nucleation limit," Science 254, 829–832 (1991).
- ¹⁴P. Pavlov and V. Skripov, "Kinetics of spontaneous nucleation in strongly heated liquids," High Temp. 8, 540–545 (1970).
- ¹⁵D. W. Oxtoby, "Homogeneous nucleation: Theory and experiment," J. Phys.: Condens. Matter 4, 7627 (1992).
- ¹⁶K. K. Tanaka, H. Tanaka, R. Angélil, and J. Diemand, "Simple improvements to classical bubble nucleation models," Phys. Rev. E 92, 022401 (2015).
- 17 L. Gránásy, "Fundamentals of the diffuse interface theory of nucleation," J. Phys. Chem. 100, 10768–10770 (1996).
- ¹⁸M. Gallo, F. Magaletti, and C. M. Casciola, "Thermally activated vapor bubble nucleation: The Landau-Lifshitz-Van der Waals approach," Phys. Rev. Fluids 3, 053604 (2018).
- ¹⁹M. Gallo, F. Magaletti, D. Cocco, and C. M. Casciola, "Nucleation and growth dynamics of vapour bubbles," J. Fluid Mech. 883, A14 (2020).
- 20P. Pfeiffer, J. Eisener, H. Reese, M. Li, X. Ma, C. Sun, and C.-D. Ohl, "Thermally assisted heterogeneous cavitation through gas supersaturation," Phys. Rev. Lett. 128, 194501 (2022).
- ²¹D.-Y. Peng and D. B. Robinson, "A new two-constant equation of state," Ind. Eng. Chem. Fundam. 15, 59-64 (1976).
- 22 X. Li and D. Yang, "Determination of mutual solubility between CO₂ and water by using the Peng-Robinson equation of state with modified alpha function and binary interaction parameter," Ind. Eng. Chem. Res. 52, 13829–13838 (2013)
- ²³I. Søreide and C. H. Whitson, "Peng-Robinson predictions for hydrocarbons, CO₂, N₂, and H₂ S with pure water and NaCI brine," Fluid Phase Equilib. 77, 217–240 (1992).
- ²⁴I. H. Bell and U. K. Deiters, "On the construction of binary mixture p-x and t-x diagrams from isochoric thermodynamics," AIChE J. 64, 2745–2757 (2018).
- 25 R. Battino, T. R. Rettich, and T. Tominaga, "The solubility of nitrogen and air in liquids," J. Phys. Chem. Ref. Data 13, 563–600 (1984).
- ²⁶N. S. Osborne, H. F. Stimson, E. F. Fiock, and D. C. Ginnings, "Properties of water," J. Res. Natl. Bur. Stand. 10, 1 (1933).

- ²⁷D. Sheppard, R. Terrell, and G. Henkelman, "Optimization methods for finding minimum energy paths," J. Chem. Phys. 128, 134106
- ⁽²⁰⁰⁶⁾.
 ²⁸B. Li, Y. Gu, and M. Chen, "An experimental study on the cavitation of water with dissolved gases," Exp. Fluids 58, 164 (2017).
- 29S. Mukherjee and H. Gomez, "Understanding how non-condensable gases modify cavitation mass transfer through the van der Waals theory of capil-
- larity," Appl. Phys. Lett. 117, 204102 (2020).

 30S. Mukherjee and H. Gomez, "Flow and mixing dynamics of phase-transforming multicomponent fluids," Appl. Phys. Lett. 115, 104101 (2019).